Diagnosing Northern Hemisphere Jet Portrayal in 17 CMIP3 Global Climate Models: Twenty-First-Century Projections

SHARON C. DELCAMBRE

Department of Atmospheric and Oceanic Sciences, and Nelson Institute Center for Climatic Research, University of Wisconsin–Madison, Madison, Wisconsin

DAVID J. LORENZ

Nelson Institute Center for Climatic Research, University of Wisconsin–Madison, Madison, Wisconsin

DANIEL J. VIMONT

Department of Atmospheric and Oceanic Sciences, and Nelson Institute Center for Climatic Research, University of Wisconsin–Madison, Madison, Wisconsin

JONATHAN E. MARTIN

Department of Atmospheric and Oceanic Sciences, University of Wisconsin–Madison, Madison, Wisconsin

(Manuscript received 18 June 2012, in final form 5 November 2012)

ABSTRACT

The anthropogenic climate change impacts on the eddy–jet system include an intensified midlatitude jet stream and an elevated tropopause, as well as a poleward-shifted jet. While both responses are evident in phase 3 of the Coupled Model Intercomparison Project (CMIP3) ensemble mean twenty-first-century projections, uncertainty in the poleward shift response is large enough that even the sign of the shift is not consistent among all models, especially in the Northern Hemisphere. The present analysis finds that twenty-first-century projections of the ensemble mean zonal wind change at 300 hPa predict a weakening and poleward expansion of the Pacific jet and an overall expansion of the Atlantic jet. In contrast with the direct zonal mean climate change signal of increasing midlatitude upper-level winds, zonal winds are projected to decrease in the core of the Pacific and Atlantic jets, with increasing zonal winds located primarily in the jet exit regions and the meridional flanks of the jets. Uncertainties in SST changes from the twentieth century to the twenty-first century between models are shown to impact modeled Northern Hemisphere jet stream changes. In particular, El Niño–Southern Oscillation–like mean winter SST changes explain 30% of intermodel variance of midlatitude zonal wind compared to the 8% explained by the domain-averaged warming SST signal. This suggests that a reduction of uncertainty in the tropical Pacific SST response to global warming will significantly reduce uncertainty in the Northern Hemisphere zonal wind response to climate change.

1. Background

Understanding how jet streams will change in the future is of primary importance in the assessment of anthropogenic climate change impacts. Jet stream position and intensity affect regional climates across the midlatitudes, perhaps predominantly through links to the midlatitude storm tracks. Dynamical theory and climate model projections suggest that the jet stream will become more intense and shift poleward under global warming. The present study examines changes in the Northern Hemisphere (NH) jet streams in a suite of global climate models to determine the robustness of these changes among models.

Increased atmospheric carbon dioxide concentrations cause the troposphere to warm and the stratosphere to cool. The troposphere warms because of increased

Corresponding author address: Sharon C. Delcambre, Department of Atmospheric and Oceanic Sciences, University of Wisconsin–Madison, 1225 W. Dayton St., Madison, WI 53706.
E-mail: scjaffe@uwalumni.com

DOI: 10.1175/JCLI-D-12-00359.1

absorption and reemission of longwave radiation due to the greenhouse effect. The stratosphere cools as increased longwave emission to space outweighs warming caused by the absorption of shortwave radiation by stratospheric ozone. The combined effect of tropospheric warming and stratospheric cooling decreases the static stability in the vicinity of the tropopause (as well as in the entire atmospheric column) and raises the height of the tropopause (Held 1993; Lorenz and DeWeaver 2007).

Also, despite the well-known surface polar amplification of the global warming temperature increase (Manabe and Stouffer 1980; Serreze et al. 2009), the atmospheric column is warming more in the tropics than the poles (i.e., as measured by thickness increases), enhancing the pole–equator temperature gradient in the midlatitudes. This is because air parcels in the tropics are constrained by radiative–convective equilibrium to follow a moist adiabatic lapse rate, leading to enhanced heating in the upper-tropospheric tropics compared to the midlatitudes because of latent heat release (Held 1993).

Both the downward slope of the tropopause from the equator to the poles and the thermal wind relationship dictate that a raised tropopause and enhanced pole–equator temperature gradient cause an intensification of the midlatitude jet streams. Therefore, the direct effects of anthropogenic climate change include higher and more intense jet streams (Kushner et al. 2001; Lorenz and DeWeaver 2007). In addition to the direct effects of climate change, a poleward shift of the jet streams has been simulated by climate models (Yin 2005; Johanson and Fu 2009; Lu et al. 2007; Wu et al. 2010; Lorenz and DeWeaver 2007; Kushner et al. 2001) and predicted statistically and dynamically.

The fluctuation–dissipation theorem (FDT), first applied to climate science by Leith (1975), relates a system's forced response to that same system's unforced internal modes of variability, assuming that climate perturbations are small enough for linear dynamics to hold (Ring and Plumb 2008). On the basis of FDT, it has been hypothesized that the jet streams will shift meridionally under anthropogenic climate change as the forced climate change signal manifests as the amplification of the northern and southern annular modes (NAM/SAM), which are the dominant modes of hemispheric variability on a monthly time scale (Ring and Plumb 2008; Gerber et al. 2008a). Studies have found that the time scale of the NAM/SAM is too long in GCM simulations (Gerber et al. 2008a), causing the modeled extratropical jet to be too sensitive to global warming perturbations (Gerber et al. 2008b).

In observations, the NAM and SAM have trended positive over the latter half of the twentieth century, indicating a poleward shift of the polar jet in both hemispheres (Thompson et al. 2000; Marshall 2003). However, the magnitude of this trend is currently in question because the annular mode has become significantly less positive since 2000 (Overland and Wang 2005). Also, a recent study suggests that using the sea level NAM/SAM, as is common practice, is ineffectual to describe jet shifts because it does not take into account the baroclinic structure of the anthropogenic climate change signal (Woollings 2008).

A future poleward shift of the midlatitude jet streams has also been explained dynamically by considering the interactions between changes in the zonal mean jet and the midlatitude eddies. One implication of the increased jet wind speeds due to the direct effects of climate change is the increase of midlatitude eddy phase speeds. The faster the eddy phase speed, the less the waves deviate from the jet core throughout their life cycle, causing the critical latitude to move poleward.[1] This shifts the associated eddy momentum fluxes produced during wave breaking poleward, resulting in a poleward shift of tropospheric winds on the equatorward flank of the jet (Chen and Held 2007; Chen et al. 2007; Lu et al. 2008).

Another dynamical mechanism suggested to be responsible for the poleward shift of the jets is the projected increase in the spatial scale of midlatitude eddies due to the decrease in overall static stability under global warming, as confirmed by GCM projections (Kidston et al. 2010). According to eddy dynamics, this increased spatial scale will cause a decrease in eddy phase speed with respect to mean tropospheric winds in the eddy source region at the jet core. Because slower eddies can travel farther before wave breaking occurs, these larger eddies will be more likely to propagate from the eddy source region before dissipating, increasing net wave propagation out of the source region (Kidston et al. 2011). Kidston et al. (2011) argue that this causes less eddy dissipation/wave breaking on the poleward side of the jet, making it more of a source region on average and suggesting a poleward expansion of the jet. Although it is possible that this mechanism will cause the entire jet to shift poleward, it is also possible that it will result in a broader jet (Kidston et al. 2011).

A simpler mechanism proposes that because the tropical atmosphere is constrained to be moist adiabatic, tropospheric dry static stability will increase more on the equatorward flank of the jet than on the poleward flank,

[1] This argument assumes that waves tend to propagate equatorward and that future zonal winds will increase more in the jet core than at the flanks of the jet.

reducing baroclinicity on the equatorward flank of the jet. A decrease of baroclinicity decreases the number of waves generated in that region, decreasing the westerly forcing on the equatorward flank of the jet (Lu et al. 2010).

However, as described in the first part of this study (Delcambre et al. 2013), the portrayal of jet stream winds in the World Climate Research Programme's (WCRP) Coupled Model Intercomparison Project phase 3 (CMIP3) multimodel dataset (Meehl et al. 2007) still lacks consensus with regard to modeled twentieth-century jet stream structure, especially in the Northern Hemisphere (Lorenz and DeWeaver 2007; Kushner et al. 2001; Kidston and Gerber 2010; Woollings and Blackburn 2012; Yaocun and Daqing 2011; Ihara and Kushnir 2009). The previous study focused on determining the reliability and robustness of nonzonally averaged NH jet stream portrayal in 17 GCMs from the CMIP3 dataset (Delcambre et al. 2013). That analysis finds significant biases in the upper-level wintertime zonal wind compared to the observed variability of upper-level winds. These wind biases are strongly related to El Niño–Southern Oscillation (ENSO)-like wintertime tropical Pacific SST biases that explain 21% of the total NH intermodel variance of the midlatitude jet stream.

As a complement to the twentieth-century analysis, the present study examines modeled NH jet streams to discover what underlies the significant intermodel variability among twenty-first-century projections. The present paper is organized as follows. Section 2 outlines the GCM data used in this study. Results of a detailed analysis of twenty-first-century jet streams in GCM simulations are presented in section 3. These results include an examination of intermodel variations related to both internal modes of variability and tropical SSTs. Conclusions are found in section 4.

2. Data and methods

The present study investigates twenty-first-century NH jet stream structure in 17 GCMs from the WCRP's CMIP3 multimodel dataset (Meehl et al. 2007). Table 1 lists the models included in this study. These particular models are chosen because they provide the daily resolved data required for this study.

The twentieth-century GCM data are produced by the climate of the twentieth-century experiment, and the twenty-first-century data employ the A1B scenario from the Intergovernmental Panel on Climate Change's Special Report on Emissions Scenarios (Nakicenovic 2000). The A1B scenario models the twenty-first century as a time of rapid economic growth and the rapid introduction of new energy technologies that are balanced between fossil fuel and nonfossil fuel sources. Population peaks midcentury in the A1B scenario, making it one of the midrange scenarios used in the CMIP3 model experiments.

Analysis is performed on daily 300- and 700-hPa zonal wind and monthly sea surface temperature (SST) for the change from the twentieth to the twenty-first century. Daily zonal wind data are smoothed using a 5-day running mean for the period encompassing 1 November–31 March of each winter from November 1979 to March 1999 and November 2081 March 2099 (with leap days removed). The 17 GCMs vary in resolution from 1.125° latitude × 1.125° longitude (model 1, INGV-SXG) to 4° latitude × 5° longitude (model 17, INM-CM3.0). To facilitate a straightforward comparison, each model is linearly interpolated to 2.5° latitude × 2.5° longitude resolution.

To create the mean winter zonal wind (SST) for the twentieth and twenty-first centuries, the smoothed (monthly) data were averaged over November–March (NDJFM) and over all 20 years of each data period. The seasonal cycle of zonal wind is created by averaging each pentad over all 20 boreal winter seasons. Smoothed daily wind data (with the seasonal cycle removed) are used to perform empirical orthogonal function (EOF)/principal component (PC) analysis.

3. Results and discussion

a. 300-hPa zonal wind change from the twentieth to the twenty-first century

To understand why GCMs do not project a consistent representation of twenty-first-century NH jet stream structure, the ensemble mean and standard deviation of the change in zonal wind from the twentieth century to the twenty-first century (1980–99 to 2081–2100, from here on referred to as the ''change in zonal wind'') are inspected and then examined in the context of internal and external system forcings.

Although the present study does not focus on a zonal mean perspective of wind speed changes in GCM projections, sectorial zonal means of the Pacific (100°–300°E) and Atlantic (240°–360°E) regions are shown in Fig. 1 to connect the present study with the larger background of work on this topic. Figures 1a and 1b show the mean model twentieth-century winter (NDJFM, 1980–99) Pacific and Atlantic zonal mean jets. Zonal mean winds are maximized in the upper troposphere and are stronger in the Pacific than in the Atlantic. The mean winter westerlies penetrate into the lower troposphere in both regions.

Figures 1c and 1d show the ensemble mean change of the winter zonal mean zonal wind. The two regions show

TABLE 1. CMIP3 models.

Number	Model	Modeling group	Reference
1	Instituto Nazionale di Geofisica e Vulcanologia Scale Interaction Experiment (INGV-SXG)	Instituto Nazionale di Geofisica e Vulcanologia	Gualdi et al. (2006, 2008)
2	Model for Interdisciplinary Research on Climate 3.2, high-resolution version [MIROC3.2 (hires)]	Center for Climate System Research (University of Tokyo), National Institute for Environmental Studies, and Frontier Research Center for Global Change [Japan Agency for Marine–Earth Science and Technology JAMSTEC)]	Hasumi and Emori (2004)
3	CSIRO Mark version 3.0 (CSIRO-Mk3.0)	Commonwealth Scientific and Industrial Research Organization (CSIRO) Atmospheric Research	Gordon et al. (2002)
4	CSIRO Mark version 3.5 (CSIRO-Mk3.5)	CSIRO Atmospheric Research	Gordon et al. (2002)
5	ECHAM5/Max Planck Institute Ocean Model (ECHAM5/MPI-OM)	Max Planck Institute for Meteorology	Jungclaus et al. (2006)
6	GFDL Climate Model version 2.0 (GFDL-CM2.0)	U.S. Department of Commerce/ National Oceanic and Atmospheric Administration (NOAA)/ Geophysical Fluid Dynamics Laboratory (GFDL)	Delworth et al. (2006) and Gnanadesikan et al. (2006)
7	BCCR Bergen Climate Model version 2.0 (BCCR-BCM2.0)	Bjerknes Center for Climate Research (BCCR)	http://www.bjerknes.uib.no/
8	Third-generation Coupled Global Climate Model with T-63 spectral resolution [CGCM3.1 (T63)]	Canadian Centre for Climate Modeling and Analysis	Flato et al. (2000) and http://www.ec.gc.ca/ccmac-cccma
9	CNRM Coupled Global Climate Model version 3 (CNRM-CM3)	Météo-France/Centre National de Recherches Météorologiques (CNRM)	http://www.cnrm.meteo.fr/scenario2004/paper_cm3.pdf
10	Model for Interdisciplinary Research on Climate 3.2, medium-resolution version [MIROC3.2 (medres)]	Center for Climate System Research (University of Tokyo), National Institute for Environmental Studies, and Frontier Research Center for Global Change (JAMSTEC)	Hasumi and Emori (2004)
11	MRI Coupled General Circulation Model version 2.3.2 (MRI-CGCM2.3.2)	Meteorological Research Institute (MRI)	Yukimoto et al. (2006)
12	Flexible Global Ocean–Atmosphere–Land System Model gridpoint version 1.0 (FGOALS-g1.0)	State Key Laboratory of Numerical Modeling for Atmospheric Sciences and Geophysical Fluid Dynamics (LASG)/Institute of Atmospheric Physics	Yu et al. (2002, 2004)
13	Third-generation Coupled Global Climate Model with T-47 spectral resolution [CGCM3.1 (T47)]	Canadian Centre for Climate Modeling and Analysis	Flato et al. (2000) and http://www.ec.gc.ca/ccmac-cccma
14	ECHAM and the global Hamburg Ocean Primitive Equation (ECHO-G)	Meteorological Institute of the University of Bonn, Meteorological Research Institute of KMA, and Model and Data group	http://www-pcmdi.llnl.gov/ipcc/model_documentation/ECHO-G.htm
15	GISS Atmosphere–Ocean Model (GISS-AOM)	National Aeronautics and Space Administration (NASA) Goddard Institue for Space Studies (GISS)	Russell et al. (1995) and Lucarini and Russell (2002)
16	GISS Model E-R (GISS-ER)	NASA GISS	Schmidt et al. (2006)
17	INM Coupled Model version 3.0 (INM-CM3.0)	Institute for Numerical Mathematics (INM)	Volodin and Diansky (2004) and Galin et al. (2003)

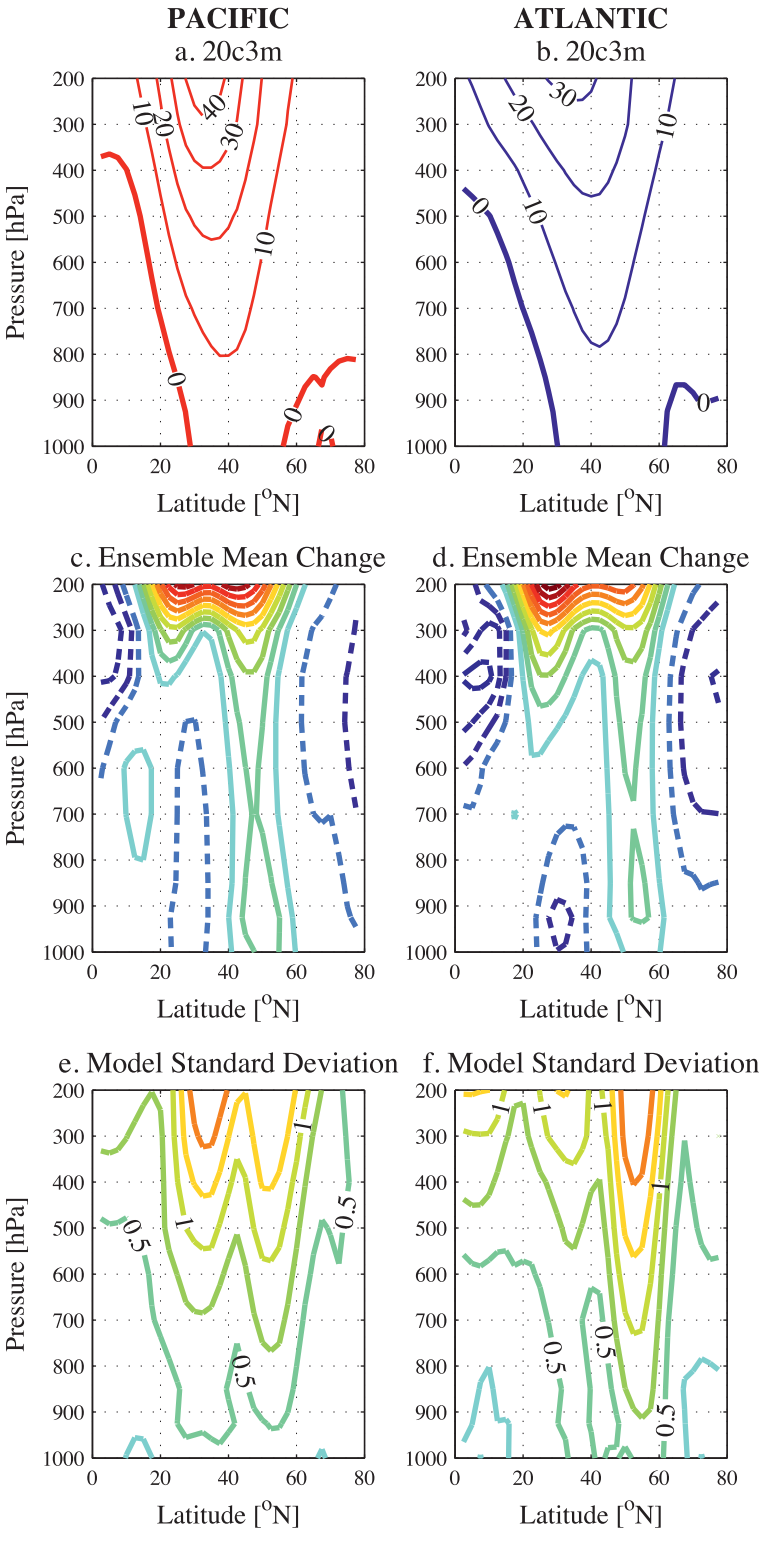

FIG. 1. Pressure (hPa) vs latitude (°N) cross sections showing modeled zonal mean zonal wind. (left) The Pacific region is averaged over 100°–300°E, and (right) the Atlantic region is averaged over 240°E–360°. (a),(b) Ensemble mean twentieth-century zonal mean zonal wind, contoured every 10 m s^{-1}. (c),(d) Ensemble mean change of the zonal mean zonal wind, contoured every 0.25 m s^{-1}, with negatives dashed and the zero line removed. (e),(f) Standard deviation of model change of the zonal mean zonal wind about the ensemble mean, contoured every 0.25 m s^{-1}.

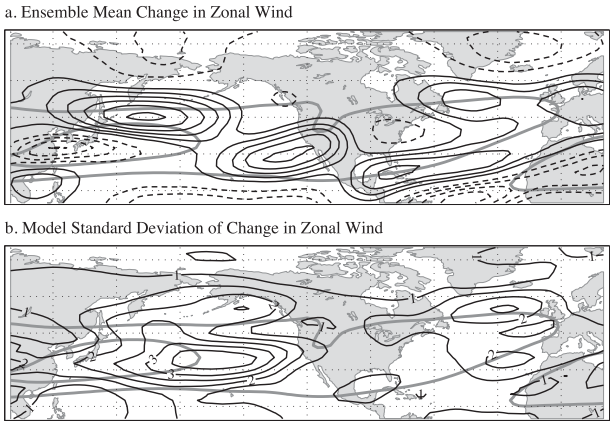

FIG. 2. (a) Ensemble mean change of the 300-hPa zonal wind from the twentieth to the twenty-first century, with solid (dashed) lines indicating positive (negative) isotachs, contoured every 0.5 m s^{-1} and with the zero line removed. (b) Standard deviation of model change in zonal wind about the ensemble mean for the 17 GCMs under consideration, contoured every 0.5 m s^{-1}. The gray contours show the 20 and 40 m s^{-1} isotachs of the ensemble mean winter 300-hPa zonal wind for the twentieth century.

similar structures of change that are characterized by an intensification of upper-level wind speeds and a northward (poleward) shift of the low-level winds associated with the jet stream. This increase in upper winds is consistent with the theorized direct response to anthropogenic climate change described in section 1. The standard deviation of the change of the winter zonal mean wind from the ensemble mean (Figs. 1e,f) is relatively small at upper levels and large at lower levels compared to the ensemble mean change (Figs. 1c,d). This suggests that the upper-level jet intensification in the region of maximum winds is much more robust than the low-level poleward shift of the jet among models. Because the maximum wind speeds are found in the upper levels of the troposphere, the present study will further analyze the modeled 300-hPa zonal winds in order to determine what underlies intermodel discrepancies in twenty-first-century projections.

The nonzonally averaged ensemble mean change in the winter 300-hPa zonal wind is shown in Fig. 2a. The twentieth-century ensemble mean zonal wind at 300-hPa is superimposed in gray. The twentieth-century climatology shows that the wintertime zonal wind is maximized in the Pacific and Atlantic basins, with the Pacific jet extending from East Asia across the Pacific basin and the Atlantic jet extending from the central continental United States toward the west coast of Europe, tilting northeastward across the Atlantic basin.

In the Pacific region, the ensemble mean change in zonal wind is largest on the poleward flank of the Pacific jet (Fig. 2a) and accompanied by a region of decreasing zonal winds in the vicinity of the jet entrance region. This asymmetric pattern looks different than the theorized poleward shift of the jet because the decrease in zonal wind is collocated with the jet axis, suggesting a poleward expansion and slight weakening of the Pacific jet in the ensemble mean. Wind speeds also increase over the eastern subtropical Pacific. In the Atlantic region, zonal winds are projected to increase poleward, equatorward, and downstream of the jet core, suggesting an overall expansion of the Atlantic jet in the ensemble mean (Fig. 2a) (Woollings et al. 2012).

It is interesting to note that in contrast to the direct climate change signal of increasing midlatitude upper-level winds (i.e., Fig. 1), the 300-hPa ensemble mean zonal winds are projected to decrease in the core of both the Pacific and Atlantic jets. This decrease in ensemble mean zonal wind is possibly related to the thermally forced weakening of the subtropical winds near 30°–35°N proposed by Chen et al. (2013). Increasing 300-hPa ensemble mean zonal winds are located primarily in the jet exit regions as well as on the meridional flanks of the jets. This is one instance in which a nonzonally averaged perspective supplements the analysis substantially.

The ensemble mean is somewhat misleading in the 17 GCMs under consideration with regard to the changes in jet stream structure in the twenty-first century. The standard deviation of the model change in zonal wind (Fig. 2b) shows that in many areas of the globe, the magnitude of the model standard deviation of wind speed change is the same or larger than the ensemble mean itself, indicating that models do not hold a unified view of the future. In particular, the standard deviation is large in the vicinity of the Pacific and Atlantic jet exit regions.

Internal jet variability is also maximized in the jet exit region (Delcambre et al. 2013), suggesting a link between model differences in changes in zonal wind and the internal modes of jet variability. Previous studies have also suggested this link; it has been hypothesized that anthropogenic climate change may project onto the natural internal modes of variability (Ring and Plumb 2008; Gerber et al. 2008a). A normalized projection of each model's change in zonal wind at 300 and 700 hPa onto the first and second EOFs of the twentieth-century zonal wind at the same level and in the same model is used to quantify the relationship between wind speed changes and internal variability. This analysis is done separately for the Pacific (100°E–120°W) and Atlantic (120°W–20°E) regions, shown for 300 hPa in Figs. 3a and 3b and for 700 hPa in Figs. 3c and 3d. The position of each point with respect to the x axis (y axis) shows the value of each model's projection onto EOF 1 (EOF 2). The

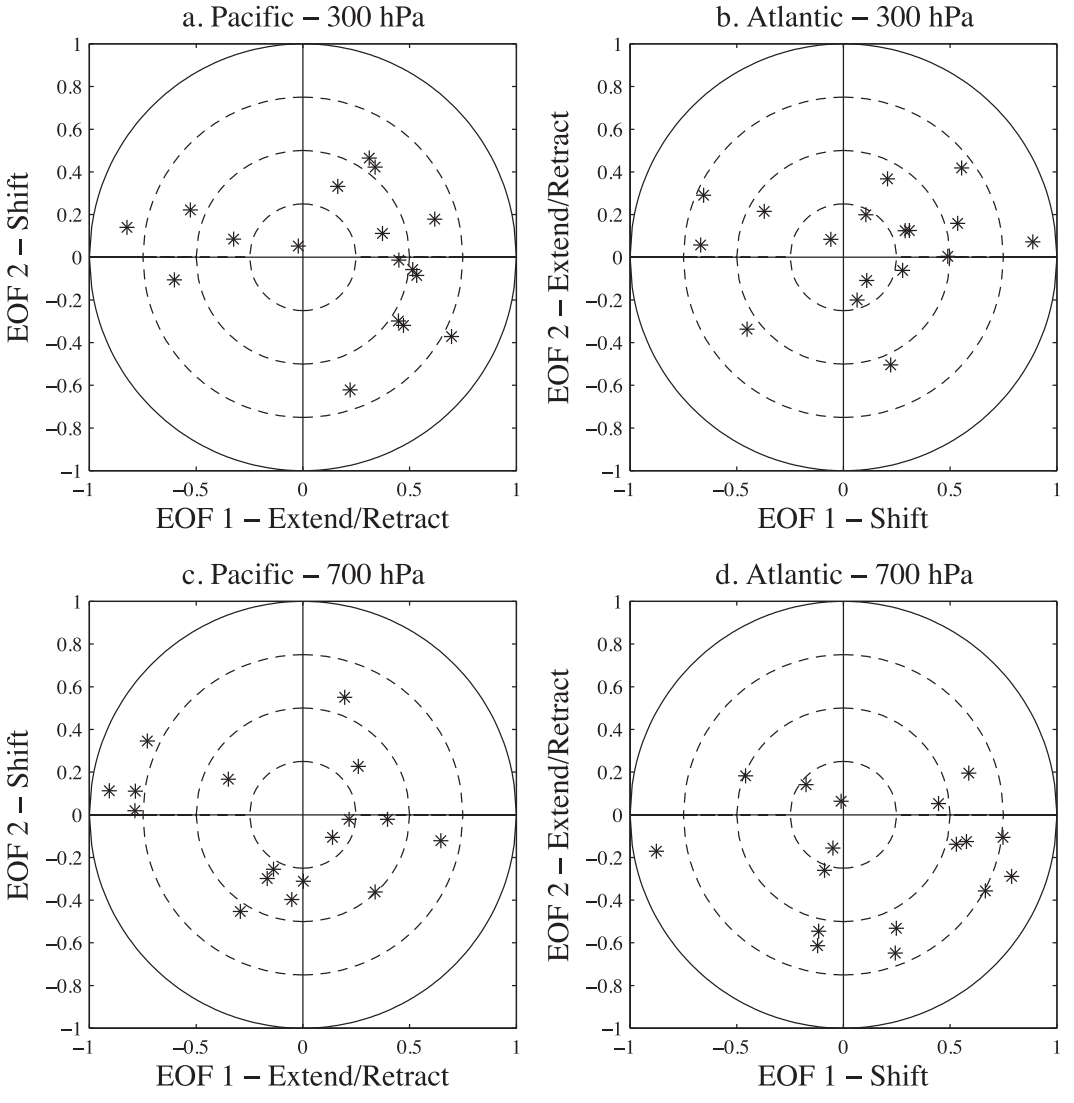

FIG. 3. Normalized projection of the model change in zonal wind from the twentieth to the twenty-first century onto EOFs 1 and 2 of the twentieth-century zonal wind from the same model for the (a) 300-hPa Pacific basin, (b) 300-hPa Atlantic basin, (c) 700-hPa Pacific basin, and (d) 700-hPa Atlantic basin. Dashed circles indicate lines of constant projection at 0.25, 0.5, and 0.75.

companion paper (Delcambre et al. 2013) shows that modeled EOFs 1 and 2 are accurate in nearly all GCMs included in this study. In both the Pacific (Figs. 3a,c) and the Atlantic (Figs. 3b,d), at 300 and 700 hPa, the values of the normalized projection are spread more along the x axis than the y axis, indicating that EOF 1 explains more variation in wind speed change among models than EOF 2. Unlike previous hypotheses suggest, however, there is no consistent projection of the change in wind onto either sign of the internal modes of variability at either level.

This analysis technique also makes it possible to quantify the relationship between the modeled change in winds and the predicted poleward shift of the jet, which can be described mathematically as $-du/dy$ for small shifts (Kushner et al. 2001). Although the results are not shown, the secondary (primary) mode of variability of the Pacific (Atlantic) jet is qualitatively similar to a poleward shift of the jet (Delcambre et al. 2013); therefore, the y axis (x axis) of Figs. 3a and 3c (Figs. 3b,d) can be replaced with $-du/dy$ to see if a poleward shift is a better predictor of zonal wind changes than EOFs 1 and 2. This analysis also shows a lack of consistent projection of the change in wind onto $-du/dy$ for each basin (not shown).

b. *Relationship between wind speed changes and tropical Pacific SSTs: MCA*

On the basis of the results of the companion paper, which found that mean winter tropical Pacific SST

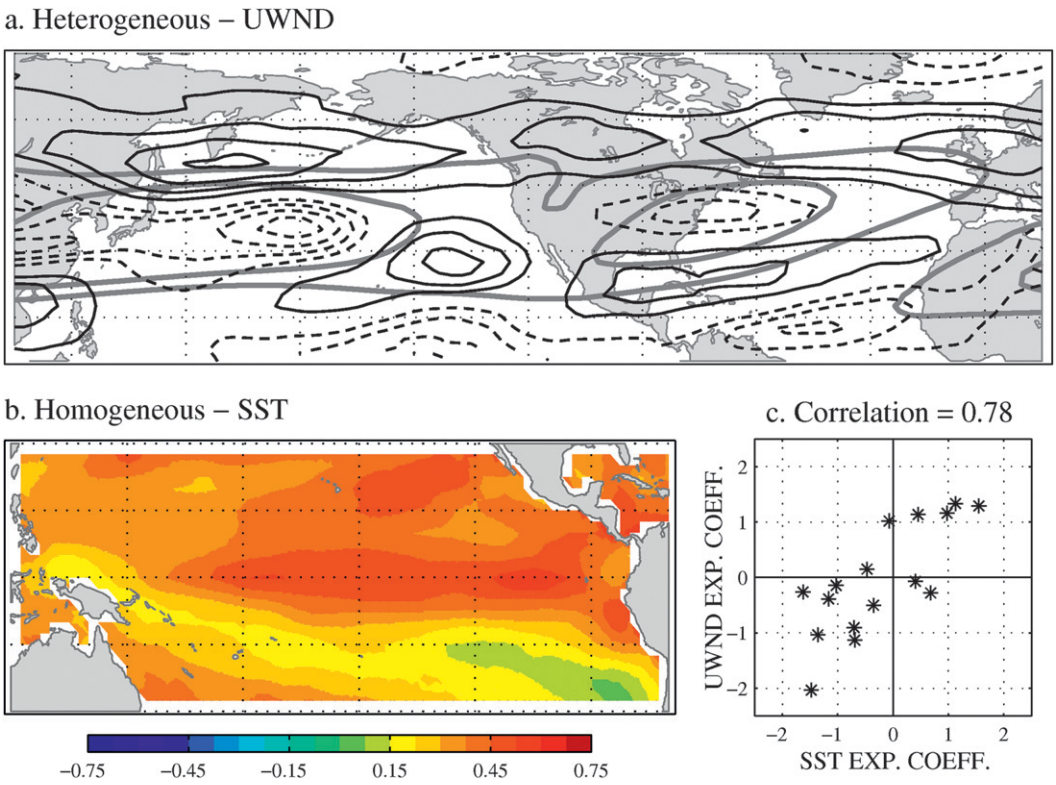

FIG. 4. Results of MCA of tropical Pacific SST change and midlatitude 300-hPa zonal wind change from the twentieth to the twenty-first century (with model 2 removed). (a) Heterogeneous zonal wind change regression map, (b) homogeneous SST change regression map, and (c) scatterplot of the wind and SST expansion coefficients. Black solid (dashed) contours in (a) represent positive (negative) perturbation isotachs contoured every 0.25 m s^{-1} (with the zero line removed), and gray contours in (a) show the 20 and 30 m s^{-1} isotachs of the ensemble mean 300-hPa zonal wind for the twentieth century.

variations explain much of the intermodel jet bias in twentieth century (Delcambre et al. 2013), it seems possible that tropical Pacific SST changes influence modeled wind speed changes more than the internal modes of atmospheric variability. Maximum covariance analysis (MCA) is used to investigate this relationship.

MCA is used here to assess the dominant patterns of covariability between tropical SSTs and the change in zonal wind from the twentieth to the twenty-first century across the same 17 GCMs. This technique identifies pairs of patterns that maximize the squared covariance between two variables: in this case, the midlatitude 300-hPa zonal wind speed change (10°–80°N, 100°E–20°W) and the tropical Pacific SST change (30°S–30°N, 120°–290°E). The covariance is identified across a given sampling dimension. Typically sampling is performed across time, but in this case sampling is done across the 17 GCMs to identify structures linked to model discrepancies. Further explanation of MCA may be found in Bretherton et al. (1992), Wallace et al. (1992), Deser and Timlin (1997), and Delcambre et al. (2013). It is important to note that because this MCA analysis samples across model space instead of across time, ENSO-like SST change patterns that are identified are not equivalent to interannual variability in any model. Instead, these ENSO-like patterns of SST change show the change in the winter mean state of the tropical Pacific from the twentieth century to the twenty-first century that is associated with a given mode of intermodel covariability.

MCA is performed three times for the 300-hPa zonal wind change, with the results shown in Figs. 4, 5, and 7. Table 2 includes the details of each case and the results of pertinent significance tests, which show that the first mode of covariability is robust in each case.

The patterns of covariability produced by MCA are depicted via regressing SST change (homogeneous pattern; Figs. 4b, 5b, and 7b) and zonal wind (UWND) change (heterogeneous pattern; Figs. 4a, 5a, and 7a) onto the SST expansion coefficient. Regression onto the zonal wind expansion coefficient yields similar structures. Here we focus on the SST expansion coefficient as a potential predictor of zonal wind change, although we do not test for causality in this study. A scatterplot of the SST and zonal

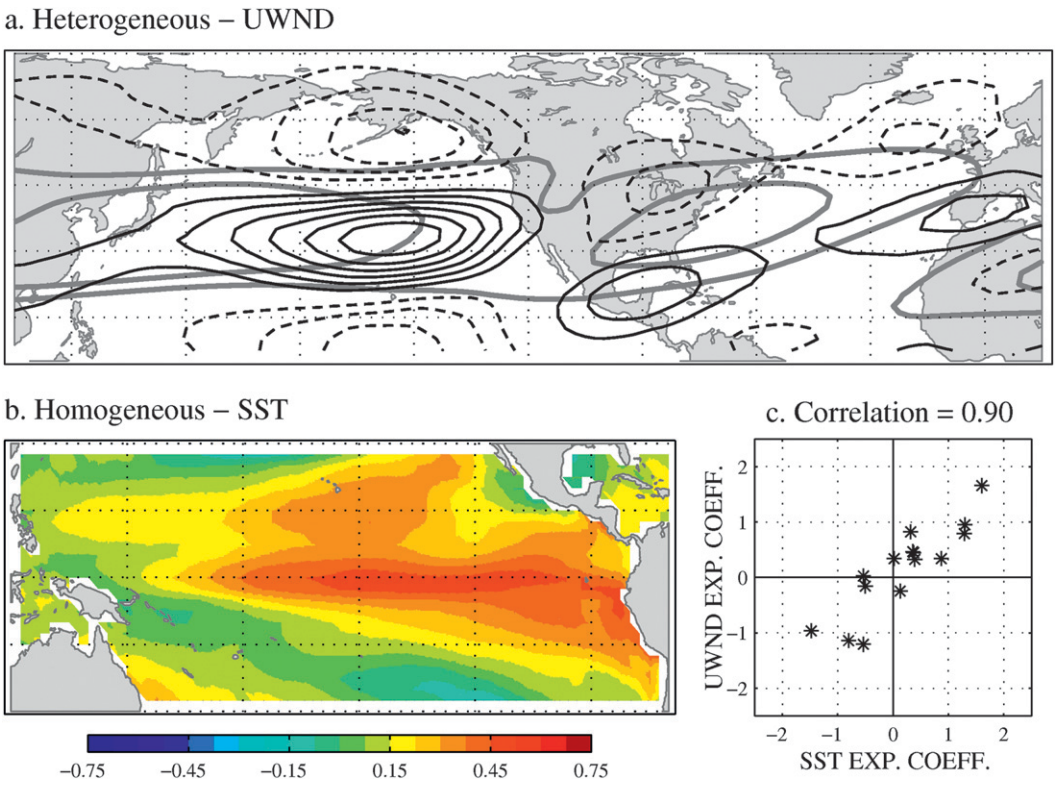

FIG. 5. As in Fig. 4, but with domain-averaged SST change removed and perturbation isotachs contoured every 0.5 m s^{-1}.

wind expansion coefficients is depicted in Figs. 4c, 5c, and 7c and demonstrates their strong correlation in each case.

1) MCA_FULL: 300-HPA ZONAL WIND CHANGE AND TROPICAL PACIFIC SST CHANGE

The first pattern of covariability between tropical Pacific SST change and 300-hPa zonal wind change is shown in Fig. 4, with the heterogeneous wind change pattern shown in Fig. 4a and the homogeneous SST change pattern shown in Fig. 4b. Model 2 [MIROC3.2 (hires)] has been removed from the analysis for MCA_Full because its SST warming from the twentieth century to the twenty-first century is much larger than all other models and significantly changes the first mode of covariability. Model 2 is an outlier for this case only and therefore is included in all other analyses.

The homogeneous SST change field (Fig. 4b) shows warming SSTs throughout the entire tropical Pacific basin. Enhanced warming in the eastern equatorial Pacific is reminiscent of the positive phase of ENSO and spatially correlated with ENSO variability in the observed record (Fig. 6b, observed ENSO) at $r = 0.47$ and the ensemble mean SST change (not shown) at $r = 0.88$. The heterogeneous wind change pattern (Fig. 4a) shows a structure of change that is similar to the ensemble mean wind speed change shown in Fig. 2a, including a poleward expansion and weakening of the Pacific jet and a meridional expansion of the Atlantic jet. The heterogeneous wind change pattern exhibits a high spatial correlation with the ensemble mean wind speed change ($r = 0.70$), but less so with the standard deviation of wind speed change ($r = 0.52$). The absolute value of the heterogeneous wind change pattern is used in the spatial correlation with the standard deviation of zonal wind change because of the absolute magnitude of variance that is used to calculate the standard deviation. To gain further insight into the intermodel variation of the change in winds, modeled ENSO-like tropical Pacific mean state changes are separated from the warming SSTs and MCA is repeated.

2) MCA_NOGW: 300-HPA ZONAL WIND CHANGE AND TROPICAL PACIFIC SST CHANGE (MEAN SST CHANGE REMOVED)

To remove the global warming signal from the tropical Pacific SSTs, the domain-averaged SST change is removed from the raw SST change field in each model prior to performing MCA_noGW (where noGW indicates that the global warming signal has been removed from the raw SST change data). The resulting pattern of covariability, shown in Fig. 5, represents the pattern of

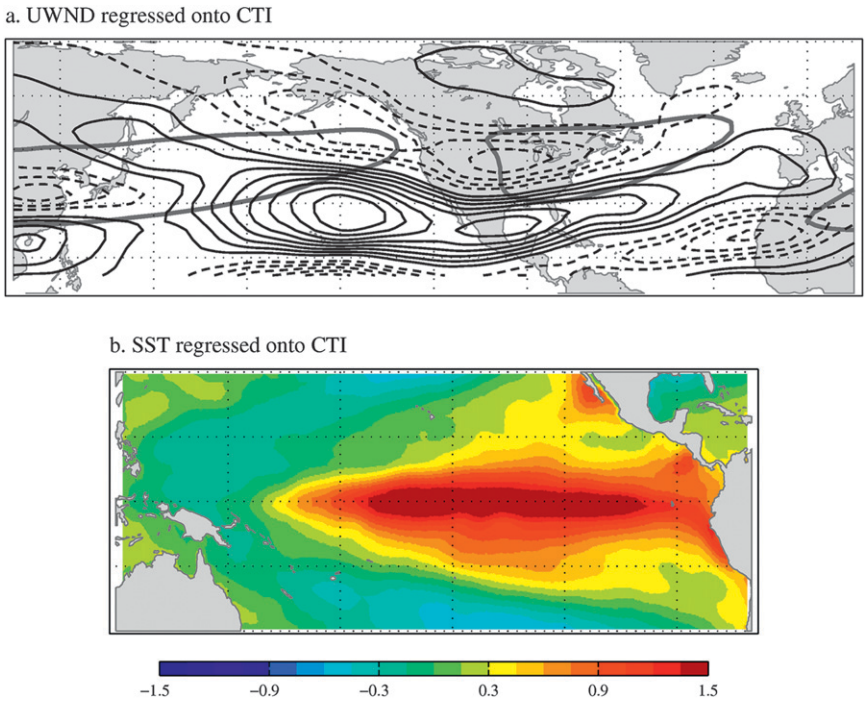

FIG. 6. ENSO midlatitude wind teleconnection (1950–2009) shown by (a) observed mean winter 300-hPa zonal wind regressed onto the mean winter CTI and (b) mean winter tropical Pacific SST regressed onto the mean winter CTI. Solid (dashed) black contours in (a) represent positive (negative) perturbation isotachs, contoured every 0.5 m s^{-1}, with the zero line removed. Gray contours represent the 20 and 40 m s^{-1} isotachs of the 300-hPa mean zonal wind.

zonal wind change that is not associated with domain-averaged warming SSTs.

In this case, the homogeneous SST change pattern (Fig. 5b) strongly resembles a positive ENSO pattern and is highly correlated with the observed mean winter ENSO SST pattern, shown in Fig. 6b ($r = 0.77$). Figure 6 shows the regression of the reanalysis winter average (NDJFM, annually resolved) zonal wind and winter average SST fields onto the reanalysis wintertime cold tongue index (CTI),[2] representing the observed patterns of winter average SST and upper-level zonal wind associated with a positive ENSO event. This homogeneous SST change pattern also strongly resembles the homogeneous SST bias pattern identified in the first part this study (Fig. 8b from Delcambre et al. 2013), suggesting that this ENSO-like SST pattern is strongly linked with both midlatitude wind biases and changes from the twentieth to the twenty-first century.

The heterogeneous wind change pattern (Fig. 5a) less strongly resembles the ensemble mean zonal wind change ($r = 0.42$) and is characterized by increased wind speeds in the Pacific jet exit region. It also strongly resembles the heterogeneous wind bias pattern from the first part of this study (Fig. 8a from Delcambre et al. 2013). A southward shift of the Atlantic jet near the jet entrance and exit regions is also present. The heterogeneous wind pattern has many similarities to the ENSO midlatitude wind teleconnection pattern from the reanalysis, particularly near the Atlantic jet entrance region (Fig. 6a), but the two patterns are not strongly spatially correlated ($r = 0.45$).

The (absolute value of the) heterogeneous wind change pattern is more highly spatially correlated with the model standard deviation of zonal wind change than in MCA_Full, with $r = 0.78$, suggesting that changes in model SSTs similar to ENSO-like structures of tropical Pacific SST change are partially responsible for intermodel variations in the portrayal of midlatitude zonal wind change. The dominant mode of intermodel variability of the 300-hPa zonal wind (i.e., EOF 1, not shown) is spatially correlated with the heterogeneous wind pattern of MCA_noGW at $r = 0.75$, further implying that a connection exists between the modeled sign of ENSO changes and midlatitude zonal wind changes.

[2] The CTI (Zhang et al. 1997) is defined by the SST anomaly pattern over the eastern equatorial Pacific (6°S–6°N, 180°–90°W) for 1950–2009.

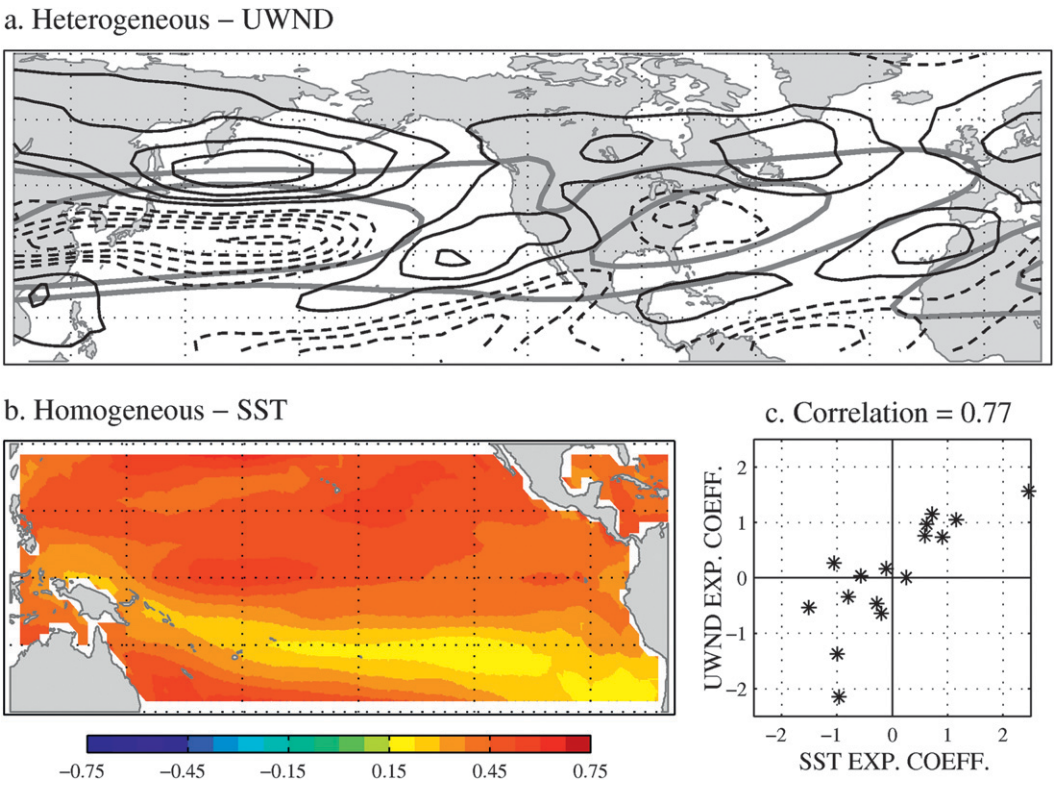

FIG. 7. As in Fig. 4, but with ENSO-like signal removed.

3) MCA_noENSO: 300-hPa zonal wind change and tropical Pacific SST change [winter mean ENSO (MCA_noGW) removed]

Next, the ENSO-like change signal in the mean winter tropical SSTs is removed from the SST field in order to examine the effects of warming SSTs on midlatitude zonal wind speed changes in the models. The MCA_noGW heterogeneous zonal wind change pattern is removed from each model's raw wind field, weighted by the standardized wind expansion coefficient for each model. MCA_noGW is used to represent the mean winter ENSO-like SST change pattern because it is highly spatially

TABLE 2. MCA analysis.

MCA	Description	Figure	Squared covariance fraction (1, 2, 3)	Normalized RMS covariance	Correlation of SST, wind expansion coefficients
MCA_Full	Tropical Pacific SST change (full) and 300-hPa zonal wind change	Fig. 4	53%, 28%, 10%	0.28	0.78
MCA_noGW	Tropical Pacific SST change (mean SST change removed) and 300-hPa zonal wind change	Fig. 5	56%, 17%, 11%	0.31	0.90
MCA_noENSO	Tropical Pacific SST change [winter mean ENSO (MCA_noGW) removed] and 300-hPa zonal wind change	Fig. 7	84%, 8%, 3%	0.31	0.77
MCA_Full_700	Tropical Pacific SST change (full) and 700-hPa zonal wind change	Not shown	62%, 22%, 6%	0.27	0.61
MCA_noGW_700	Tropical Pacific SST change (mean SST change removed) and 700-hPa zonal wind change	Not shown	55%, 17%, 10%	0.30	0.90
MCA_noENSO_700	Tropical Pacific SST change [winter mean ENSO (MCA_noGW_700) removed] and 700-hPa zonal wind change	Not shown	87%, 5%, 2%	0.31	0.76

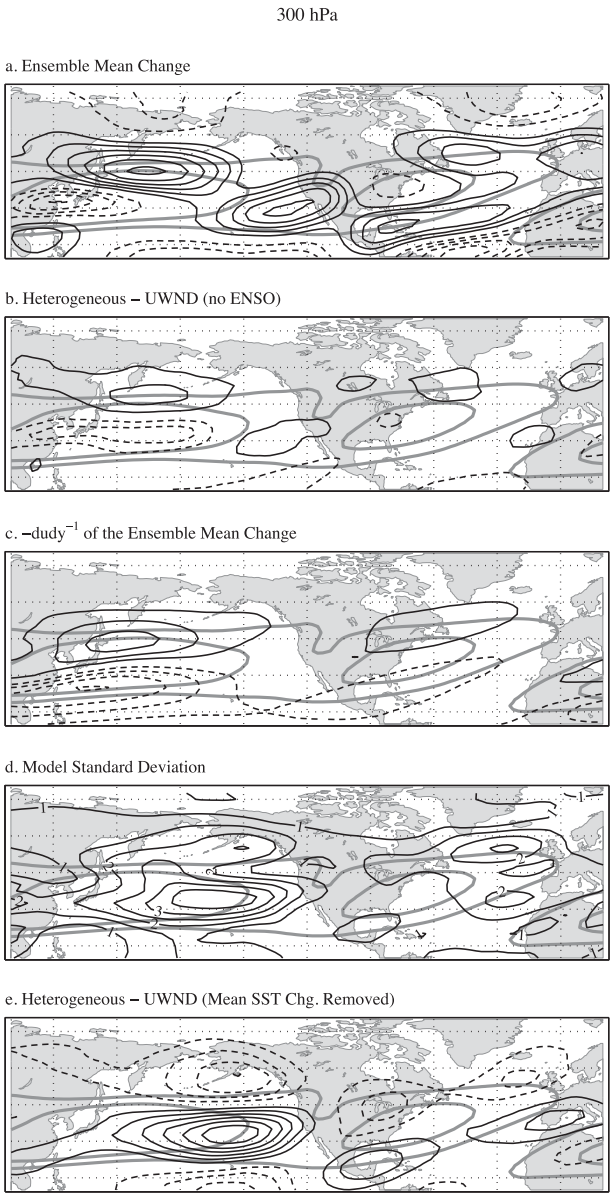

FIG. 8. (a) Ensemble mean change of the 300-hPa zonal wind, (b) heterogeneous zonal wind change regression map (ENSO-like signal removed, as in Fig. 7a), (c) $-du/dy$ of the ensemble mean twentieth-century zonal wind, (d) standard deviation of the change in zonal winds about the ensemble mean, and (d) heterogeneous zonal wind change regression map (with domain-averaged SST change removed, as in Fig. 5a), all at 300 hPa. The gray lines show the 20 and 30 m s^{-1} contours of the ensemble mean twentieth-century winds at 300 hPa. In all panels black solid (dashed) contours represent positive (negative) perturbation isotachs contoured every 0.5 m s^{-1} [1 s^{-1} in (c)] with the zero line removed.

correlated with the observed mean winter ENSO signal. The same method is used for SST: the homogeneous SST change pattern weighted by each model's standardized SST expansion coefficient is removed from each model's raw SST change field. This process is intended to remove the mean winter ENSO-like signal in each model, weighting the amount of pattern removed by the relative magnitude of the ENSO-like mean SST change pattern in each model. The results of this analysis are shown in Fig. 7.

The homogeneous SST change pattern (Fig. 7b) shows warming everywhere in the tropical Pacific and is not spatially correlated with the observed ENSO pattern ($r = 0.05$, not shown). It is spatially correlated with the ensemble mean SST change at $r = 0.56$. The heterogeneous zonal wind change pattern (Fig. 7a) resembles the heterogeneous wind change field of MCA_Full and is correlated with the ensemble mean zonal wind change at $r = 0.70$ and the absolute value of the model standard deviation at $r = 0.59$. The heterogeneous zonal wind change pattern (Fig. 7a) shows a northward expansion and weakening of the Pacific jet and a less pronounced northward expansion and weakening of the Atlantic jet. It also shows increased winds in the eastern Pacific, consistent with the ensemble mean change shown in Fig. 2a. Therefore, the relative warming of mean winter SSTs in each model is related to the northward expansion and weakening of the modeled NH jets.

To clarify and emphasize the results from the three prior analyses, Fig. 8 summarizes the main findings from MCA of the upper-level zonal wind and SST changes across models. A summary of the spatial correlation between the panels of Fig. 8 is found in Table 3. Figure 8b shows the heterogeneous zonal wind change field of the mean winter SST change with the ENSO-like change signal removed (MCA_noENSO; Fig. 7a). This wind field is spatially correlated with the ensemble mean zonal wind change (Fig. 8a) at $r = 0.70$, signifying that the zonal wind change related to global warming SSTs strongly resembles the ensemble mean zonal wind change. This warming zonal wind change (Fig. 8b) is spatially correlated with $-du/dy$ (Fig. 8c, a poleward shift of the jet) at $r = 0.30$, while the ensemble mean zonal wind change is spatially correlated with $-du/dy$ at $r = 0.17$. Therefore, removing the ENSO-like change signal of MCA_noGW presents a signal that more strongly resembles a poleward shift of the jet, even if it still is not highly correlated with a poleward shift pattern.

Figure 8e shows the heterogeneous zonal wind change pattern of the mean winter SST change with the domain-averaged SST change removed (MCA_noGW; Fig. 5a). As mentioned above, the absolute value of this pattern is spatially correlated with the model standard deviation (Fig. 2b) at $r = 0.78$, indicating that the ENSO-like change signal is strongly related to intermodel variations in jet stream portrayal. In addition, the fact that the ensemble mean SST change (not shown) shows enhanced

TABLE 3. MCA correlations.

Variable 1	Variable 2	Spatial correlation (300 hPa)	Spatial correlation (700 hPa)
Ensemble mean change	Heterogeneous zonal wind (no ENSO)	0.70	0.78
Ensemble mean change	$-\frac{du}{dy}$	0.17	0.48
Heterogeneous zonal wind (no ENSO)	$-\frac{du}{dy}$	0.30	0.28
Model standard deviation	Heterogeneous zonal wind (no mean SST change)	0.39	0.44
Model standard deviation	Magnitude of heterogeneous zonal wind (no mean SST change)	0.78	0.79

warming in the eastern equatorial Pacific, reminiscent of an El Niño event, most likely contributes to changes in midlatitude winds. The combination of these analyses suggests that the mean winter ENSO-like change signal of SST variations across models as well as the ensemble mean positive ENSO signal may be masking the poleward shift of the jet in the ensemble mean. This point will be discussed further in section 4.

4) A COMPARISON AT 700 HPA

MCA is repeated for the tropical Pacific SST change and 700-hPa zonal wind change. Figure 9 summarizes the results of a parallel three-part analysis at 700 hPa (details in Tables 2, 3). Overall, the results of MCA using the 700-hPa change in zonal wind are very similar to the analysis at 300 hPa. Figure 9b shows the heterogeneous zonal wind field of the mean winter SST change with the ENSO-like signal removed (MCA_noENSO_700). The heterogeneous zonal wind change pattern is correlated with the ensemble mean zonal wind change (Fig. 9a) at $r = 0.78$. In this case the zonal wind change related to warming SSTs resembles the ensemble mean zonal wind change even more strongly than at 300 hPa. This warming zonal wind change is correlated with $-du/dy$ (Fig. 9c, a poleward shift of the jet) at $r = 0.28$, while the ensemble mean zonal wind change is correlated with $-du/dy$ at $r = 0.48$.

Figure 9e shows the heterogeneous zonal wind change pattern of the mean winter SST change with the domain-averaged SST change removed (MCA_noGW_700). The absolute value of this pattern is spatially correlated with the 700-hPa model standard deviation (not shown) at $r = 0.79$, again suggesting that the ENSO-like change signal is strongly related to model variations in jet stream changes from the twentieth to the twenty-first century.

c. *Relationship between wind speed changes and tropical Pacific SSTs: Regression analysis*

Using MCA, the ENSO-like SST change signal and warming SST signal have been separated statistically (section 3b). To verify the results of MCA, an independent investigation is performed using regression analysis. The winter mean CTI change is calculated for each model, as well as the domain-averaged SST change from the twentieth to the twenty-first century for the global tropical ocean (27.5°S–27.5°N, 0°–360°). In this analysis, the CTI change from the twentieth century to the twenty-first century is examined with the domain-averaged SST change removed.

The zonal wind change is regressed onto the mean SST change in each model, and the resulting pattern, shown in Fig. 10a, resembles both the ensemble mean zonal wind change (shown in red) and the heterogeneous zonal wind change pattern from MCA_noENSO (Fig. 7a). The regression field is correlated with those patterns at $r = 0.80$ and $r = 0.95$, respectively, and shows a weakening and northward expansion of the Pacific jet, increased wind speeds in the eastern Pacific, and a slight expansion of the Atlantic jet. This pattern is not highly spatially correlated with the model standard deviation (Fig. 2b, $r = 0.57$). Thus, the modeled warming of SSTs is again shown to be related to the poleward expansion and weakening of the Pacific jet, and a slight expansion of the Atlantic jet, although the signal in the Atlantic is very small in comparison.

When the zonal wind change is regressed onto the CTI change (with the domain-averaged SST change removed) in each model (Fig. 10b), the positive wind speed anomaly in the vicinity of the jet exit region strongly resembles the model standard deviation of wind speed change, and the two fields are highly correlated ($r = 0.78$). This result agrees with the assertion from MCA_noENSO that changes in mean winter SSTs resembling ENSO-like tropical Pacific SSTs are partially responsible for the variation among models in jet stream portrayal, especially in the Pacific.

d. *Intermodel variance*

To quantify how much the modeled ENSO-like pattern of winter SST change explains variations in jet

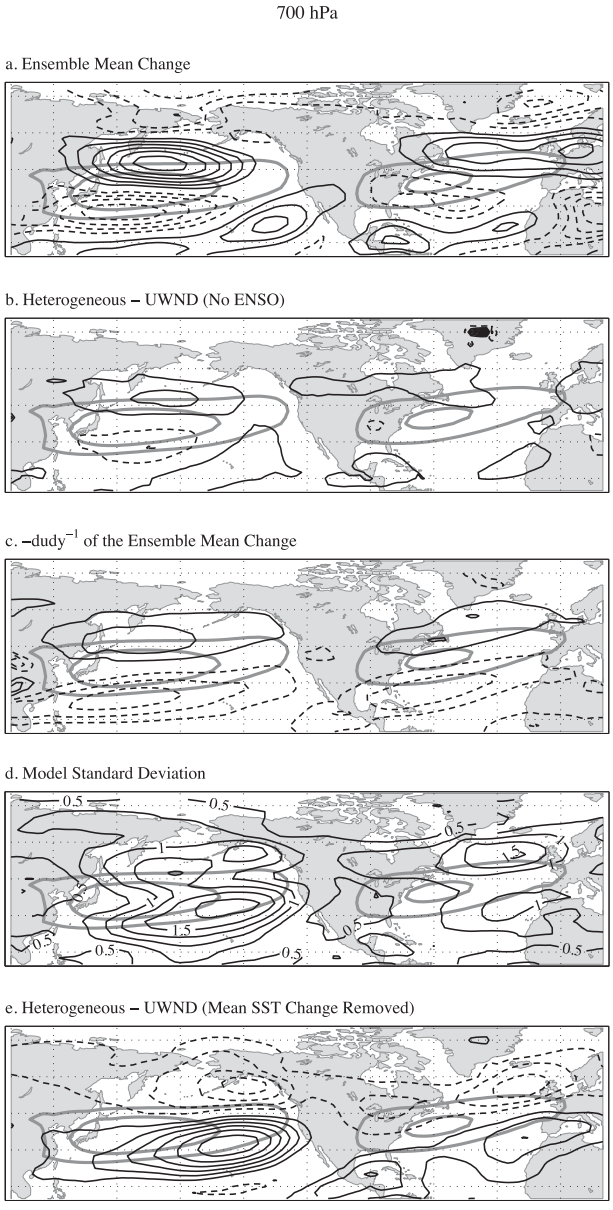

FIG. 9. As in Fig. 8, but for 700-hPa zonal wind. The gray lines show the 10, 15, and 20 m s^{-1} contours of the ensemble mean twentieth-century winds at 700 hPa. In all panels black solid (dashed) contours represent positive (negative) perturbation isotachs contoured every 0.25 m s^{-1} [0.5 s^{-1} in (c)] with the zero line removed.

portrayal among models, Fig. 11 examines the intermodel variance of zonal wind changes from the twentieth to the twenty-first century. The intermodel variance is highest in the central Pacific, with a secondary region of variance found in the Northern Atlantic region (Fig. 11a). Using the SST expansion coefficients from MCA_noGW and MCA_noENSO as predictors of intermodel variance, the amount of variance explained by each of these patterns

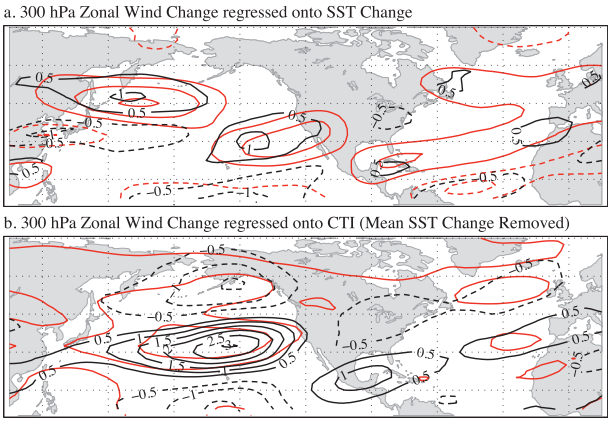

FIG. 10. The modeled change in 300-hPa zonal winds (m s^{-1}) regressed onto (a) global tropical SST change for each model and (b) model CTI (with mean global tropical SST change removed). Black solid (dashed) contours represent positive (negative) perturbation isotachs contoured every 0.5 m s^{-1} (with the zero line removed), and red contours in (a) show the ensemble mean change and in (b) show the standard deviation of the zonal wind change at 300-hPa, contoured every 1 m s^{-1}.

can be calculated using regression analysis. The variance explained by MCA_noGW and the linear combination of MCA_noGW and MCA_noENSO are shown in Figs. 11b and 11c, respectively.

While 8% of domain-averaged intermodel variance is explained by warming SSTs (not shown), 30% is explained by the ENSO-like signal in each model (Fig. 11b). In the Pacific basin, the ENSO-like SST signal explains 40% of the variance, while in the Atlantic this signal only explains 13% of the total variance. In the central subtropical Pacific region where intermodel variance is maximized, nearly all of the variance is explained by intermodel variations in the ENSO-like pattern of mean winter SST changes. On the basis of this result, it seems that, if the mean winter change in ENSO from the twentieth to the twenty-first century was more robust in GCMs, it would be possible to significantly improve NH jet stream characterization, especially in the Pacific region.

4. Conclusions

This study has analyzed changes in NH zonal winds from the twentieth to the twenty-first century from a nonzonal mean perspective. The ensemble mean zonal wind change at 300 hPa shows a weakening and poleward expansion of the Pacific jet and an overall expansion of the Atlantic jet. These structures are distinct from the theorized poleward shift of the jet and do not consistently project onto internal modes of variability at 300 or 700 hPa, as suggested by previous studies.

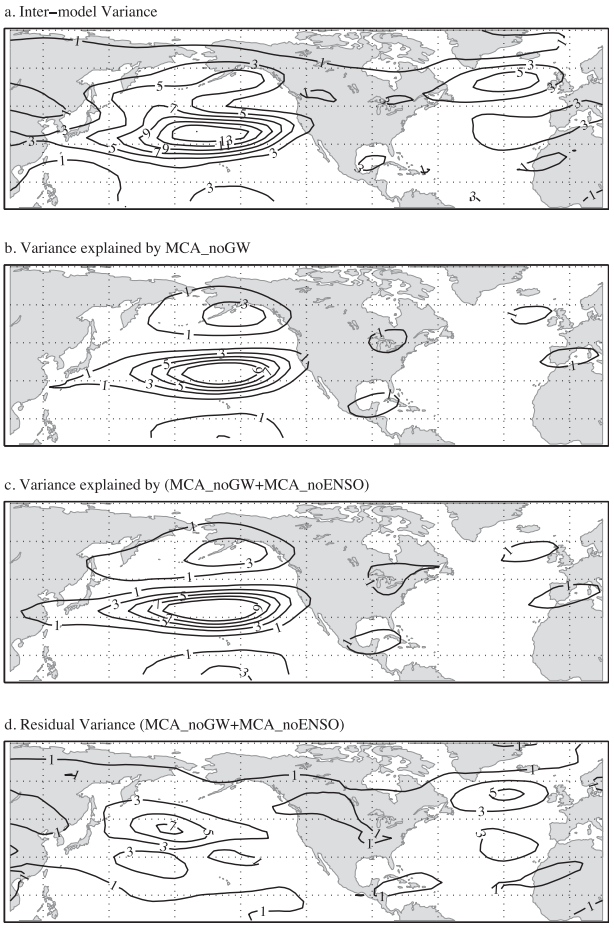

FIG. 11. (a) Total intermodel variance of the change in the winter 300-hPa zonal wind from the twentieth century to the twenty-first century. Intermodel variance explained by (b) MCA_noGW, (c) linear combination of MCA_noGW and MCA_noENSO, and (d) residual of MCA_noGW and MCA_noENSO. Variance is contoured every 2 $m^2\ s^{-2}$, starting at 1 $m^2\ s^{-2}$.

It is important to note that models project varying changes in zonal winds at different levels of the atmosphere. While expansion and weakening are projected of winds in the upper troposphere, the ensemble mean shows a poleward shift of winds in the lower troposphere (with relatively large standard deviation). The dissimilarity between levels suggests that the distinct influences of the subtropical and polar jet should be an area of research focus in order to characterize the response of each jet to anthropogenic climate change. It is also interesting to note that, in contrast with the direct climate change signal of increasing midlatitude upper-level winds (i.e., Fig. 1), ensemble mean 300-hPa zonal winds are projected to decrease in the core of both the Pacific and Atlantic jets. Increasing 300-hPa zonal winds are located primarily in the jet exit regions, as well as on the meridional flanks of the jets.

A statistical examination of the link between mean winter SST changes and zonal wind changes shows that SST differences between models impact the model portrayal of NH jet stream changes, particularly in the Pacific region. In particular, ENSO-like mean winter SST changes explain 30% of intermodel variation, compared to the 8% explained by the domain-averaged warming SST signal identified by MCA and confirmed through regression analysis. This suggests that refining the sign of ENSO changes and its midlatitude teleconnection patterns in GCMs will increase confidence in the use of models to understand midlatitude jet stream features under anthropogenic climate change.

As in the first part of this study, we have assumed that tropical SSTs are responsible for forcing midlatitude winds, suggesting that the variation in models' portrayal of tropical Pacific SST changes contributes to the discrepancies among modeled midlatitude large-scale circulation changes. This hypothesis is consistent with prior research detailing ENSO teleconnection patterns (e.g., Lau 1997; Trenberth et al. 1998; Seager et al. 2003). However, it is important to note that the reverse scenario is also possible. It is possible for midlatitude and subtropical winds to produce tropical Pacific SST variations, such as by the seasonal footprinting mechanism (Vimont et al. 2001). Although the present study does not prove any direction of causality, the patterns depicted in the results do suggest that model variations in tropical Pacific SST changes are influencing the intermodel variability of midlatitude zonal wind changes.

The broad similarity between the ensemble mean zonal wind changes and the zonal wind changes predicted by warming SSTs in MCA is promising. Even though varying model portrayals of the change of the mean winter ENSO-like tropical Pacific SSTs strongly affect zonal wind changes, there is a large model spread around the ensemble mean, although some enhanced warming in the eastern equatorial Pacific is still evident (not shown; $r = 0.56$ with Fig. 5b). This El Niño–like signal in the ensemble mean SST change indicates that ENSO still affects the ensemble mean response in the midlatitude winds to some extent. An improvement of the consistency and accuracy of ENSO portrayal is important and will unmask previously unknown characteristics of the climate change signal in NH zonal winds. The first part of this study demonstrates that NH biases in upper-level winds are strongly related to an ENSO-like pattern of biases in winter mean tropical Pacific SSTs, also suggesting that improvements in model portrayal of the tropical Pacific mean state may significantly advance the portrayal of the mean state of the Pacific and Atlantic jets. For now, it is important to know that ENSO and SST warming are the two dominant

predictors of zonal wind changes (of the tropical SST field) in GCMs in order to correctly interpret the significance of CMIP3 model projections of zonal winds in the twenty-first century.

Finally, we put forth MCA as an advantageous tool for assessing covarying parameters across multiple GCMs. While MCA is often used to understand variables that covary temporally, this new application of MCA is a powerful way to determine intermodel reliability. We plan to continue using MCA to examine SST variations across models, investigating the relationship of SST changes and NH precipitation changes from the twentieth to the twenty-first century.

Acknowledgments. This research was supported by NSF Grant ATM-0653795, NOAA Grant NA08OAR4310880, and NSF Grant ATM-0806430. We thank the two reviewers for their insightful comments, which greatly improved the paper. In addition, we acknowledge the modeling groups, the Program for Climate Model Diagnosis and Intercomparison (PCMDI), and the WCRP's Working Group on Coupled Modelling (WGCM) for their roles in making available the WCRP CMIP3 multimodel dataset. Support of this dataset is provided by the Office of Science, U.S. Department of Energy.

REFERENCES

Bretherton, C. S., C. Smith, and J. M. Wallace, 1992: An intercomparison of methods for finding coupled patterns in climate data. *J. Climate,* **5,** 541–560.

Chen, G., and I. Held, 2007: Phase speed spectra and the recent poleward shift of Southern Hemisphere surface westerlies. *Geophys. Res. Lett.,* **34,** L21805, doi:10.1029/2007GL031200.

——, ——, and W. Robinson, 2007: Sensitivity of the latitude of the surface westerlies to surface friction. *J. Atmos. Sci.,* **64,** 2899–2915.

——, J. Lu, and L. Sun, 2013: Delineating the eddy-zonal flow interaction in the atmospheric circulation response to climate forcing: Uniform SST warming in an idealized aqua-planet model. *J. Atmos. Sci.,* **70,** 2214–2233.

Delcambre, S., D. Lorenz, D. Vimont, and J. Martin, 2013: Diagnosing Northern Hemisphere jet portrayal in 17 CMIP3 global climate models: Twentieth-century intermodel variability. *J. Climate,* **26,** 4910–4929.

Delworth, T., and Coauthors, 2006: GFDL's CM2 global coupled climate models. Part I: Formulation and simulation characteristics. *J. Climate,* **19,** 643–674.

Deser, C., and M. Timlin, 1997: Atmosphere–ocean interaction on weekly timescales in the North Atlantic and Pacific. *J. Climate,* **10,** 393–408.

Flato, G., G. Boer, W. Lee, N. McFarlane, D. Ramsden, M. Reader, and A. Weaver, 2000: The Canadian Centre for Climate Modelling and Analysis of global coupled model and its climate. *Climate Dyn.,* **16,** 451–467.

Galin, V. Y., E. M. Volodin, and S. P. Smyshliaev, 2003: Atmosphere general circulation model of INM RAS with ozone dynamics. *Russ. Meteor. Hydrol.,* **5,** 13–22.

Gerber, E., L. Polvani, and D. Ancukiewicz, 2008a: Annular mode time scales in the Intergovernmental Panel on Climate Change Fourth Assessment Report models. *Geophys. Res. Lett.,* **35,** L22707, doi:10.1029/2008GL035712.

——, S. Voronin, and L. Polvani, 2008b: Testing the annular mode autocorrelation time scale in simple atmospheric general circulation models. *Mon. Wea. Rev.,* **136,** 1523–1536.

Gnanadesikan, A., and Coauthors, 2006: GFDL's CM2 global coupled climate models. Part II: The baseline ocean simulation. *J. Climate,* **19,** 675–697.

Gordon, H., and Coauthors, 2002: The CSIRO Mk3 Climate System Model. Tech. Paper 60, CSIRO, Aspendale, Victoria, Australia, 130 pp.

Gualdi, S., E. Scoccimarro, A. Bellucci, A. Grezio, E. Manzini, and A. Navarra, 2006: The main features of the 20th century climate as simulated with the SXG coupled GCM. *Claris Newsletter,* No. 4, CLARIS Project, Buenos Aires, Argentina, 7–14. [Available online at http://eolo.cima.fcen.uba.ar/documents/newsletter/news_4_low.pdf.]

——, ——, and A. Navarra, 2008: Changes in tropical cyclone activity due to global warming: Results from a high-resolution coupled general circulation model. *J. Climate,* **21,** 5204–5228.

Hasumi, H., and S. Emori, 2004: K-1 coupled GCM (MIROC) description. K-1 Tech. Rep. 1, Center for Climate System Research, University of Tokyo, Tokyo, Japan, 34 pp. [Available online at http://www.ccsr.u-tokyo.ac.jp/kyosei/hasumi/MIROC/tech-repo.pdf.]

Held, I., 1993: Large-scale dynamics and global warming. *Bull. Amer. Meteor. Soc.,* **74,** 228–242.

Ihara, C., and Y. Kushnir, 2009: Change of mean midlatitude westerlies in 21st century climate simulations. *Geophys. Res. Lett.,* **36,** L13701, doi:10.1029/2009GL037674.

Johanson, C., and Q. Fu, 2009: Hadley cell widening: Model simulations versus observations. *J. Climate,* **22,** 2713–2725.

Jungclaus, J., and Coauthors, 2006: Ocean circulation and tropical variability in the coupled model ECHAM5/MPI-OM. *J. Climate,* **19,** 3952–3972.

Kidston, J., and E. Gerber, 2010: Intermodel variability of the poleward shift of the austral jet stream in the CMIP3 integrations linked to biases in 20th century climatology. *Geophys. Res. Lett.,* **37,** L09708, doi:10.1029/2010GL042873.

——, S. Dean, J. Renwick, and G. Vallis, 2010: A robust increase in the eddy length scale in the simulation of future climates. *Geophys. Res. Lett.,* **37,** L03806, doi:10.1029/2009GL041615.

——, G. Vallis, S. Dean, and J. Renwick, 2011: Can the increase in the eddy length scale under global warming cause the poleward shift of the jet streams? *J. Climate,* **24,** 3764–3780.

Kushner, P., I. Held, and T. Delworth, 2001: Southern Hemisphere atmospheric circulation response to global warming. *J. Climate,* **14,** 2238–2249.

Lau, N.-C., 1997: Interactions between global SST anomalies and midlatitude atmospheric circulation. *Bull. Amer. Meteor. Soc.,* **78,** 21–33.

Leith, C., 1975: Climate response and fluctuation dissipation. *J. Atmos. Sci.,* **32,** 2022–2026.

Lorenz, D., and E. DeWeaver, 2007: Tropopause height and zonal wind response to global warming in the IPCC scenario integrations. *J. Geophys. Res.,* **112,** D10119, doi:10.1029/2006JD008087.

Lu, J., G. Vecchi, and T. Reichler, 2007: Expansion of the Hadley cell under global warming. *Geophys. Res. Lett.,* **34,** L06805, doi:10.1029/2006GL028443.

——, G. Chen, and D. Frierson, 2008: Response of the zonal mean atmospheric circulation to El Niño versus global warming. *J. Climate,* **21,** 5835–5851.

——, ——, and ——, 2010: The position of the midlatitude storm track and eddy-driven westerlies in aquaplanet AGCMs. *J. Atmos. Sci.,* **67,** 3984–4000.

Lucarini, V., and G. Russell, 2002: Comparison of mean climate trends in the Northern Hemisphere between National Centers for Environmental Prediction and two atmosphere-ocean model forced runs. *J. Geophys. Res.,* **107,** 4269, doi:10.1029/2001JD001247.

Manabe, S., and R. Stouffer, 1980: Sensitivity of a global climate model to an increase of CO_2 concentration in the atmosphere. *J. Geophys. Res.,* **85,** 5529–5554.

Marshall, G., 2003: Trends in the southern annular mode from observations and reanalyses. *J. Climate,* **16,** 4134–4143.

Meehl, G., C. Covey, T. Delworth, M. Latif, B. McAvaney, J. Mitchell, R. Stouffer, and K. Taylor, 2007: The WCRP CMIP3 multimodel dataset: A new era in climate change research. *Bull. Amer. Meteor. Soc.,* **88,** 1383–1394.

Nakicenovic, N., 2000: Greenhouse gas emissions scenarios. *Technol. Forecasting Soc. Change,* **65,** 149–166.

Overland, J., and M. Wang, 2005: The Arctic climate paradox: The recent decrease of the Arctic Oscillation. *Geophys. Res. Lett.,* **32,** L06701, doi:10.1029/2004GL021752.

Ring, M., and R. Plumb, 2008: The response of a simplified GCM to axisymmetric forcings: Applicability of the fluctuation–dissipation theorem. *J. Atmos. Sci.,* **65,** 3880–3898.

Russell, G., J. Miller, and D. Rind, 1995: A coupled atmosphere–ocean model for transient climate change studies. *Atmos.–Ocean,* **33,** 683–730.

Schmidt, G., and Coauthors, 2006: Present-day atmospheric simulations using GISS ModelE: Comparison to in situ, satellite, and reanalysis data. *J. Climate,* **19,** 153–192.

Seager, R., N. Harnik, Y. Kushnir, W. Robinson, and J. Miller, 2003: Mechanisms of hemispherically symmetric climate variability. *J. Climate,* **16,** 2960–2978.

Serreze, M., A. Barrett, J. Stroeve, D. Kindig, and M. Holland, 2009: The emergence of surface-based Arctic amplification. *Cryosphere,* **3,** 11–19.

Thompson, D., J. Wallace, and G. Hegerl, 2000: Annular modes in the extratropical circulation. Part II: Trends. *J. Climate,* **13,** 1018–1036.

Trenberth, K., G. Branstator, D. Karoly, N.-C. Lau, and C. Ropelewski, 1998: Progress during TOGA in understanding and modeling global teleconnections associated with tropical sea surface temperatures. *J. Geophys. Res.,* **103,** 14 291–14 324.

Vimont, D., D. Battisti, and A. Hirst, 2001: Footprinting: A seasonal connection between the tropics and mid-latitudes. *Geophys. Res. Lett.,* **28,** 3923–3926.

Volodin, E., and N. Diansky, 2004: El-Niño reproduction in a coupled general circulation model of atmosphere and ocean. *Russ. Meteor. Hydrol.,* **12,** 5–14.

Wallace, J. M., C. Smith, and C. S. Bretherton, 1992: Singular value decomposition of wintertime sea surface temperature and 500-mb height anomalies. *J. Climate,* **5,** 561–576.

Woollings, T., 2008: Vertical structure of anthropogenic zonal-mean atmospheric circulation change. *Geophys. Res. Lett.,* **35,** L19702, doi:10.1029/2008GL034883.

——, and M. Blackburn, 2012: The North Atlantic jet stream under climate change and its relation to the NAO and EA patterns. *J. Climate,* **25,** 886–902.

——, J. Gregory, J. Pinto, M. Reyers, and D. Brayshaw, 2012: Response of the North Atlantic storm track to climate change shaped by ocean–atmosphere coupling. *Nat. Geosci.,* **5,** 313–317.

Wu, Y., M. Ting, R. Seager, H. Huang, and M. Cane, 2010: Changes in storm tracks and energy transports in a warmer climate simulated by the GFDL CM2.1 model. *Climate Dyn.,* **37,** 53–72.

Yaocun, Z., and H. Daqing, 2011: Has the East Asian westerly jet experienced a poleward displacement in recent decades? *Adv. Atmos. Sci.,* **28,** 1259–1265.

Yin, J., 2005: A consistent poleward shift of the storm tracks in simulations of 21st century climate. *Geophys. Res. Lett.,* **32,** L18701, doi:10.1029/2005GL023684.

Yu, Y., R. Yu, X. Zhang, and H. Liu, 2002: A flexible coupled ocean–atmosphere general circulation model. *Adv. Atmos. Sci.,* **19,** 169–190.

——, X. Zhang, and Y. Guo, 2004: Global coupled ocean–atmosphere general circulation models in LASG/IAP. *Adv. Atmos. Sci.,* **21,** 444–455.

Yukimoto, S., and Coauthors, 2006: Present-day climate and climate sensitivity in the Meteorological Research Institute Coupled GCM Version 2.3 (MRI-CGCM2.3). *J. Meteor. Soc. Japan,* **84,** 333–363.

Zhang, Y., J. Wallace, and D. Battisti, 1997: ENSO-like interdecadal variability: 1900–93. *J. Climate,* **10,** 1004–1020.